

## Comprehensive study of the luminescence properties of elemental metals

Tohru Suemoto<sup>1,\*</sup>, Shota Ono<sup>2,3,†</sup>, Akifumi Asahara<sup>1</sup>, Tsuyoshi Okuno<sup>1</sup>, Takeshi Suzuki<sup>4</sup>,  
Kozo Okazaki<sup>4</sup>, Shuntaro Tani<sup>4</sup>, and Yohei Kobayashi<sup>4</sup>

<sup>1</sup>Department of Engineering Science, *The University of Electro-Communications, Chofu, Tokyo 182-8585, Japan*

<sup>2</sup>Department of Sciences and Informatics, *Muroran Institute of Technology, Muroran, Hokkaido 050-8585, Japan*

<sup>3</sup>Institute for Materials Research, *Tohoku University, 2-1-1 Katahira, Aoba-ku, Sendai 980-8577, Japan*

<sup>4</sup>Institute for Solid State Physics, *The University of Tokyo, Kashiwanoha 5-1-5, Kashiwa, Chiba, Japan*

 (Received 5 June 2024; revised 21 October 2024; accepted 24 December 2024; published 27 January 2025)

The lifetime and intensity of ultrafast luminescence in the near-infrared region were investigated for 15 representative elemental metals: simple light metals (Be, Mg, and Al); *3d* (Ti, Ni, and Zn), *4d* (Zr, Mo, Pd, and Sn), and *5d* (W and Pt) transition metals; and noble metals (Au, Ag, and Cu). The luminescence intensity at 0.9 eV was distributed over a range as wide as 2.5 orders of magnitude. The sum of an instantaneous response and an exponential decay component well approximated the time-evolution of the luminescence intensity at 0.6 eV. The lifetimes obtained from this decomposition were distributed in a narrower range from 110 fs (Be) to 694 fs (Ag), corresponding to a factor 6.3. We proposed a model based on the dielectric function of the bulk metal to understand the luminescence intensity of the quasi-instantaneous component. It was found that the luminescence intensity was inversely proportional to the Drude damping constant, that is, the slower the damping, the stronger the luminescence. This shows that quasi-instantaneous luminescence is quenched by the nonradiative decay of the nonthermal electrons via electron-electron scattering. The electron-phonon (e-ph) coupling strengths were evaluated using Eliashberg functions derived from *ab initio* calculations, and the decay rates corresponding to e-ph scattering were evaluated using the extended two-temperature model considering the equilibration process of excited electrons. We found fairly good agreement between the experimental and theoretical results for the absolute values of the exponential decay rates.

DOI: [10.1103/PhysRevB.111.035150](https://doi.org/10.1103/PhysRevB.111.035150)

### I. INTRODUCTION

The study of photoluminescence in metals was initiated half a century ago by Mooradian [1], who discovered interband luminescence in bulk gold and copper under blue laser irradiation. Boyd *et al.* [2] further investigated the luminescence mechanism using well-controlled surfaces and established interband luminescence involving the *d* band for noble metals. Recently, authors have also identified the interband luminescence in Mg, which does not belong to the noble metals [3]. In addition to interband luminescence, a two-photon-induced intraband luminescence was reported by Beversluis *et al.* [4] for gold, and a cascade-type excitation mechanism for this luminescence was shown by Imura *et al.* [5]. Research progress in this field was hindered due to the associated very low quantum yield and consequent lack of applications, unlike for luminescence in semiconductors. However, luminescence from nanostructured metals has much higher intensity and has recently received increasing attention for applications in imagers or tracers in biomedicine [6–8]. Luminescence is an important tool for investigating the excited states and their dynamics in nanometer-sized metals, which function as useful catalysts and photonic devices [8].

Motivated by these applications, attempts have been made to comprehensively understand light emissions from metals [9–11].

Luminescence spectra in metals and their time-development originating from nonthermal and thermal electrons were treated theoretically [11,12]. The stepwise electron distribution characteristic to the cascade excitation predicted by the theory was verified by excitation density dependence (so-called *power-law exponent*) of luminescence intensity in Au nanorods under femtosecond pulse-train excitation [11]. This provided evidence for emission from nonthermal electrons generated by laser pulse excitation. Several reports on nanostructured metals have appeared recently. The light emission mechanism in Au nanospheres and nanorods have been studied by polarization correlation of luminescence [13]. The Purcell effect in the light emission mechanism in Au nanorods was discussed based on luminescence spectra and their excitation wavelength dependence [14]. Despite the active research in theory and experiment, understanding of metal luminescence has not been established.

Until now, the luminescence of metals has been mainly studied in noble metals in the bulk form [1,2] and in nanostructured form [4–7,15,16] with a few examples of other metals such as Pt and Pd in the form of nanometer-sized particles [8,17–20]. The preparation methods and morphologies of the samples were very different among the available

\*Contact author: suemoto@issp.u-tokyo.ac.jp

†Contact author: shotaono@muroran-it.ac.jp

reports, and a systematic review of the general behavior of the luminescence properties of metals was difficult.

Looking at this present situation, we can point out three major obstacles in research of metal luminescence from the experimental side: (i) lack of ultrafast time-resolved luminescence data, (ii) lack of information on a wide range of metals other than noble metals, and (iii) lack of studies on bulk materials free from specialized morphology. Recently, we established a method for measuring luminescence spectra with good reproducibility using intentionally roughened surfaces. Previously, we reported the ultrafast infrared luminescence of group 11 noble metals (Au, Ag, and Cu) and group 10 transition metals (Pt, Pd, and Ni) measured under nearly the same conditions [21]. The luminescence intensities and lifetimes were very different for these two groups. The lifetimes were short (on the order of 100 fs), and the intensities were significantly lower for group 10 metals than for group 11 noble metals. We qualitatively interpreted this behavior in terms of the difference in density of states (DOS) of the electrons near the Fermi surface. When the DOS is large, the electron-electron (e-e) and electron-phonon (e-ph) scattering rates increase, resulting in short lifetimes and weak luminescence. However, the size of the subgroups investigated was insufficient to discuss the general behavior of metal luminescence quantitatively.

Our preceding investigation showed that infrared luminescence originating from *intragand* transitions could be observed in many kinds of metals, including alloys and semimetals, when the surface is roughened by sandblasting or similar methods [21–23]. Although the fabricated surface morphology is not the same for every metal, the sample-dependent effect of the surface morphology can be corrected by normalizing the luminescence spectra by the absorption spectra, which are equivalent to the emissivity spectra according to Kirchhoff's law for radiation. Thus, the correct internal luminescence spectra can be obtained [23]. The inhomogeneity of the surface is further averaged out by rotating the sample during measurement, if precise and highly reproducible spectra are required. As our method is robust and general, it applies to any metal.

In this paper, we present the luminescence properties of 15 elemental metals including the aforementioned six metals. It should be noted that this paper is not a simple complement of our previous work but provides another set of information because it is essential to compare all metals under the same experimental condition. A semiempirical model was proposed to understand the elemental dependence of luminescence intensity. We performed *ab initio* calculations to evaluate e-ph interaction strength and interpret the lifetime.

## II. EXPERIMENT

We used an in-house-developed femtosecond-luminescence spectrometer based on an up-conversion technique. Mode-locked pulses with a repetition rate of 100 MHz at 1036 nm (1.19 eV) from a Yb-fiber laser were amplified to an average power of 600 mW using a Yb-fiber amplifier. Pumping pulses (typically 150 fs duration, 200 mW, 2 nJ/pulse) were focused on the sample with a spot size of 20  $\mu\text{m}$ . Assuming a typical penetration depth of 10 nm, the

transient increase of temperature is estimated to be 200 K, which is comparable with the energy of room temperature. The luminescence was collected and focused on a nonlinear optical crystal (lithium iodate) using two paraboloidal mirrors and frequency mixed with gating pulses. A Si plate was placed between the two paraboloidal mirrors close to the Brewster angle to remove anti-Stokes luminescence from the sample. The generated sum-frequency light was passed through a long-wave-pass edge filter and directed to a spectrometer consisting of tunable band-pass filters. The signal was detected using an avalanche photodiode (APD; COUNT-50N-FC, Laser Components, Germany), and the photons were registered using a frequency counter. The time resolution of this system is typically 240 fs (full width at half maximum). Our experimental setup with a photomultiplier for the detector instead of an APD is described in the supplemental material of our previous paper [22]. All luminescence measurements were performed in air at room temperature.

The absorptivity of the samples was measured at 1.19 eV as an increase of temperature under irradiation by a Yb-fiber laser with reduced power (20 mW) using an in-house-made calorimeter. The absorptivity at longer wavelengths (see the Supplemental Material [24]) was measured using an optical parametric amplifier operating at a repetition frequency of 1 kHz.

Metal samples were purchased from the Nilaco Corporation as sheets or rods. The rods were sliced into pieces of 1–2 mm thickness. The surfaces of the samples were either sandblasted or pressed with an alumina polishing film. The samples were rotated during the measurement to avoid degradation and average the inhomogeneity of roughness, except for some samples which did not have flat surfaces. The samples studied in this paper are listed in Table I in the order of their atomic number. They are categorized into five groups: light metals; 3*d*, 4*d*, and 5*d* transition metals; and noble metals. Although noble metals belong to transition metals, they are categorized separately as noble because of their special luminescence properties.

## III. RESULTS

Figure 1 shows the time evolution of luminescence intensity at 0.9 eV for eight representative metals. The data for the other metals are compiled in the Supplemental Material [24]. To reliably compare the luminescence intensities of 15 metals, we performed measurements continuously for a few days under the same conditions as far as possible. The intensity data for different days were calibrated using the luminescence intensity of Au as a standard. Namely, we measured a standard Au sample to check the total sensitivity of the measurement system just before or after a series of measurements and scaled the count rate of the samples by that of the Au standard sample. Although Cu and Ni exhibited the highest and lowest intensities, respectively, in this figure, Zr had the lowest intensity among all (Supplemental Material [24]). The maximum count rates of the time-evolution curves at 0.9 eV are tabulated in Table I [column (b)].

The luminescence efficiency is enhanced by surface roughness, and the enhancement factor critically depends on the

TABLE I. Luminescence properties of metals.

Atomic number	Element	$A$ (%) <sup>a</sup>	$I^b$	$I^c$	$\Gamma_{\text{exp}}^d$	Comments
4	Be	74.8	775	1385	9.1	Light metal
12	Mg	56.4	1366	4294	6.4	
13	Al	51.7	2424	9069	6.94	
22	Ti	92.3	72	85	8.55	3d trans.
28	Ni	81	68	104	8.619	
29	Cu	85.6	15 562	21 238	2.57	(Noble)
30	Zn	90	2446	3020	3.02	4d trans.
40	Zr	72.6	44	83	6.9	
42	Mo	71.5	448	876	8.84	
46	Pd	65.2	236	555	4.48	
47	Ag	73.9	14 373	26 318	1.44	(Noble)
50	Sn	47.5	555	2460	3.88	
74	W	71.6	218	425	4.5	5d trans.
78	Pt	58.1	594	1760	3.38	
79	Au	82.5	6594	9688	1.54	(Noble)

<sup>a</sup>Absorptivity at 1.19 eV.

<sup>b</sup>Luminescence intensity at 0.9 eV ( $I$ ).

<sup>c</sup>Emissivity corrected intensity  $I = I'/A^2$ .

<sup>d</sup>Decay rate (1/ps) defined in Eq. (1).

surface morphology. We normalized the count rate by the absorptivity at excitation and emissivity at the luminescence photon energies to avoid the uncertainty of luminescence intensity due to this surface effect. For Ag surfaces with various degrees of surface roughness, we have shown previously that the luminescence intensity at 0.9 eV under excitation at

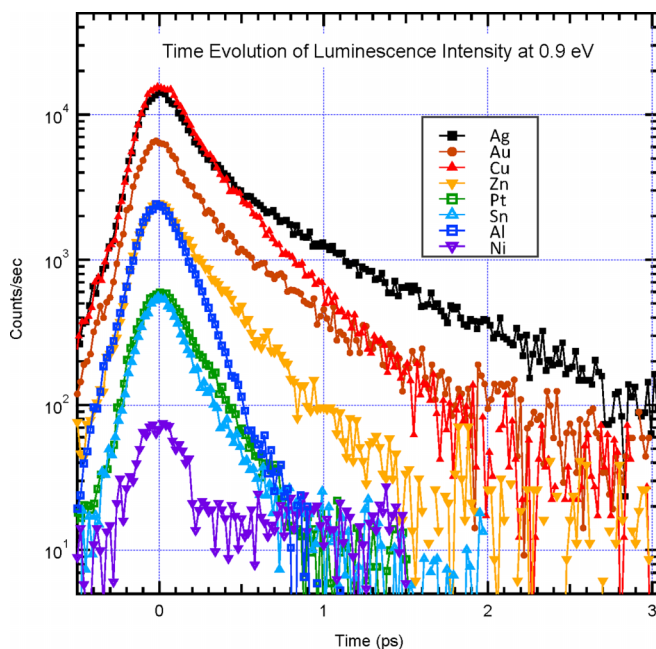


FIG. 1. Time evolution of luminescence intensity at 0.9 eV for eight representative metals (Ag, Au, Cu, Pt, Zn, Sn, Ni, and Al). The ordinate is the actual photon counting signal measured under the same experimental conditions without normalizing by emissivity. The data taken on different days are scaled using the Au signal as a standard. The data for other metals are compiled in the Supplemental Material [24].

1.19 eV is nearly proportional to the square of the absorptivity at 1.19 eV [22]. Because emissivity is a gentle function of the photon energy, we can reasonably assume the emissivity at 0.9 eV to be nearly equal to that at 1.19 eV. The absorptivities, which are equal to emissivity according to Kirchhoff's law, at 1.19 eV measured by calorimetry are listed in Table I [column (a)]. Applying the above-mentioned square law to these metals, we corrected the effect of surface morphology on the luminescence intensity and obtained the intrinsic luminescence intensity, represented as  $I$  [column (c)] in Table I. This enables a meaningful comparison of luminescence intensities of different metals. The large variation in  $I$  among the different metals, by a factor of 300, will be discussed in Sec. IV A.

Since the luminescence at 0.6 eV has a slower decay rate than that at 0.9 eV and is suitable for evaluating the lifetime, we performed measurements at 0.6 eV. Figure 2 shows the time evolution of the luminescence intensity at 0.6 eV, where the peak intensities have been normalized to 1000 counts/s for a set of metals shown in Fig. 1. To analyze these curves, we assumed a quasi-instantaneous response (expressed by a delta function) and an exponentially decaying component. The experimental curves were approximated by a convoluted response curve

$$I(t) = \int_{-\infty}^{\infty} g(t-t')[A_0 \delta(t') + A_1 \exp(-\Gamma_{\text{exp}} t')] dt', \quad (1)$$

where

$$g(t) = \frac{1}{w\sqrt{\pi}} \exp\left(-\frac{t^2}{w^2}\right) \quad (2)$$

is a normalized Gaussian function representing the instrumental response. The function  $g(t)$  for FWHM = 0.29 ps is shown by a dashed curve in Fig. 2. It properly represents the shape of the curves for a negative delay near  $t = 0$  but shows a large deviation below  $t = -0.3$  ps, where the signal is lower than the  $\frac{1}{10}$  level owing to the nonideal pulse shape of the laser.

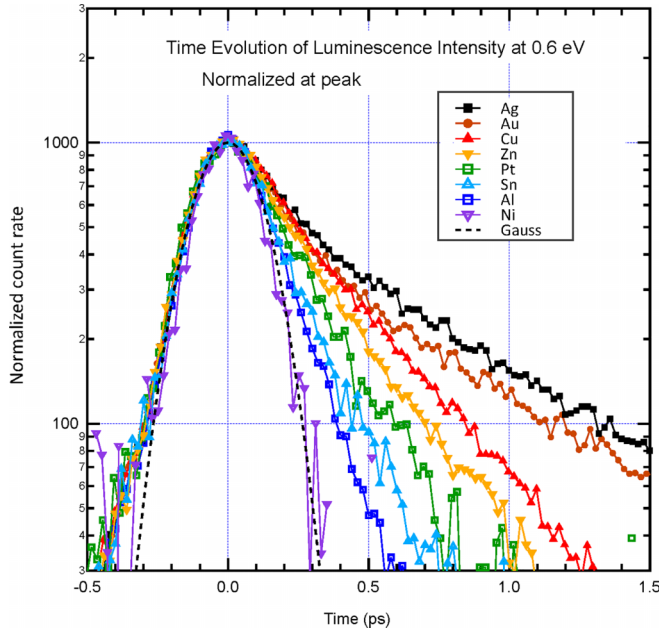


FIG. 2. Time evolution curves of luminescence intensity at 0.6 eV for eight representative metals (Ag, Au, Cu, Pt, Zn, Sn, Al, and Ni). The curves are normalized to 1000 counts/s at their maxima. The instrumental response function for full width at half maximum (FWHM) = 0.29 ps approximated by a Gaussian curve is shown by the dashed curve. The data for other metals are compiled in the Supplemental Material [24].

Therefore, we used data  $> \frac{1}{10}$  of the maximum value to fit both for the negative and positive delays. As the width of  $g(t)$  fluctuates between 0.27 and 0.30 ps from measurement to measurement, we regarded  $w$  as a variable, which was adjusted for each curve. The time evolution curves for all the metals could be well approximated using Eq. (1), and the decay rate for the exponential component  $\Gamma_{\text{exp}}$  was obtained. The decomposition procedure for Au is illustrated in Fig. 3 as an example. The decay profiles of all the metals were reproduced using this decomposition procedure with a similar fitting quality. The obtained exponential decay rates  $\Gamma_{\text{exp}}$  are listed in Table I [column (d)].

The correlation between the peak intensity  $I$  at 0.9 eV and the exponential decay rate  $\Gamma_{\text{exp}}$  is shown in Fig. 4. For metals with very short lifetimes, such as Be, Mo, Ti, and Ni, the deconvolution procedure includes a larger ambiguity because the time constant is close to the instrumental response. It is interesting to note that the data points are not distributed homogeneously but are distributed in the area above a line with a negative slope. This indicates that metals with long exponential lifetimes always exhibit high instantaneous luminescence intensities.

The physical meaning of the two components in Eq. (1) is understood as follows. As we have discussed in previous papers [21,23], the electron population can be approximated by a sum of a thermal (Fermi-Dirac) distribution  $f_{\text{FD}}(x, t)$  with an appropriate electron temperature and the nonthermal

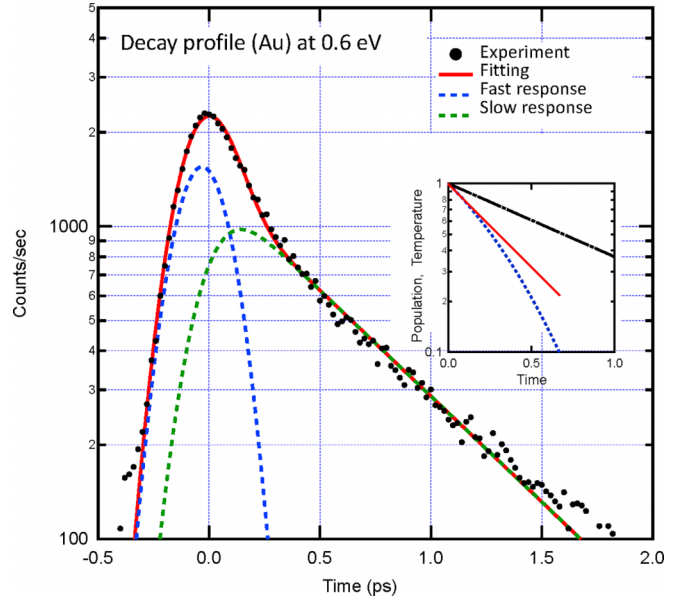


FIG. 3. Decomposition of the time evolution curves into an instantaneous response (blue dashed curve) and an exponentially decaying component (green dashed curve). This figure shows the result for Au as an example. Inset: Calculated time evolution of electron temperature,  $T(t)$  (black chain) and electron population (blue dots) at 0.6 eV for  $kT_0 = 0.24$  eV, both normalized to unity. The time axis is normalized by the cooling time constant. The red solid line shows the slope at  $t = 0$ .

distribution  $f_{\text{NT}}(x, t)$  created by optical excitation:

$$f_{\text{NT}}(x, 0) = \begin{cases} n_{\text{NT}}\theta(E_{\text{exc}} - x), & \text{for } x > 0, \\ 1 - n_{\text{NT}}\theta(E_{\text{exc}} + x), & \text{for } x < 0, \end{cases} \quad (3)$$

where  $\theta(x)$  is a unit step function,  $E_{\text{exc}}$  is the excitation photon energy 1.19 eV, and  $n_{\text{NT}}$  is the population of nonthermal electrons. Just after excitation by a short laser pulse, the electron population is dominated by  $f_{\text{NT}}(x, 0)$ , and the maximum kinetic energy of the electron reaches  $E_{\text{exc}}$ . When time elapses, the population  $f_{\text{NT}}(x, t)$  decreases from the top end. We assume that the quasi-instantaneous response corresponds to the high-energy electrons described by  $f_{\text{NT}}(x, t)$ , which disappears via e-e scattering in a very short time compared with the time resolution of the present experiment. After some time, the Fermi-Dirac distribution  $f_{\text{FD}}(x, t)$  is established, and the time evolution is well described by the cooling of the electron system emitting phonons. Of course, both processes occur at the same time and cannot be strictly separated. However, this simplification was used to see the essence of the relaxation process of excited electrons.

#### IV. DISCUSSION

The roughness on surfaces enables our samples (15 metals) to absorb and emit photons with high efficiency. This is because the surface roughness resolves the wave number mismatch between the photon in vacuum and the surface plasmon polariton (SPP) that is confined near the metal surface. For example, Ag with a heavily roughened surface shows hot luminescence that is three orders of magnitude larger than a

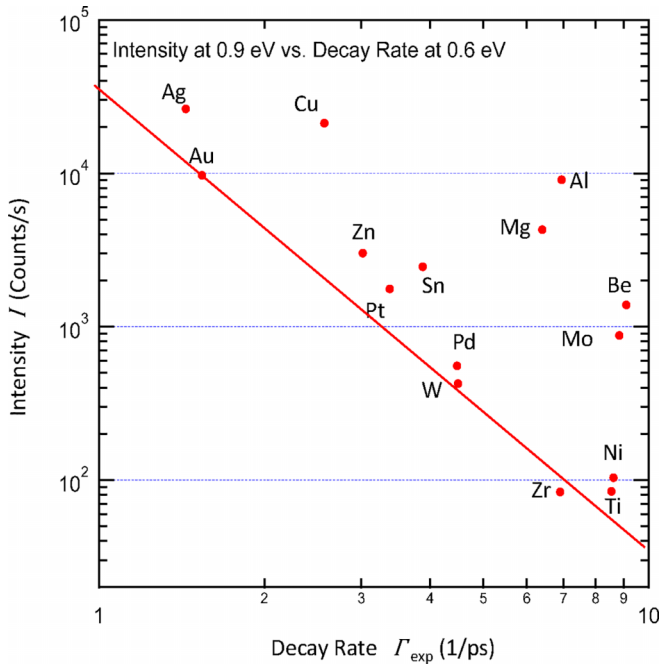


FIG. 4. Maximum internal luminescence intensities  $I$  at 0.9 eV as a function of decay rate  $\Gamma_{\text{exp}}$  at 0.6 eV (double logarithmic plot) for 15 elemental metals. The red line shows a boundary of distribution: Metals with small decay rate exhibit high luminescence intensities.

smooth surface [22]. Note also that a series of elementary processes, i.e., photon absorption, SPP propagation, and photon emission, has been studied in high-quality patterned metals [25–27], and the radiation process mediated by SPP has been established for noble metals.

In this paper, we assume that, (i) in the initial stage of relaxation, the SPP decays due to e-e scattering; (ii) in the final stage of relaxation, the SPP decays due to e-ph scattering; and most importantly, (iii) nonthermal or thermal electrons near the surface (either) form a steady state with the SPP at the moment of radiation, where the *steady state* in this paper expresses a frequent energy exchange between the SPP and excited electrons: The SPP collapses to excited electrons, and simultaneously, excited electrons are combined to create the SPP. The third assumption, which allows us to replace the SPP dynamics with the electron dynamics, is speculated from the fact that the time-resolved luminescence spectra in metals are well described by the cooling process of the electron system [21,23].

Using the frequency-dependent dielectric constant and the e-ph coupling constant, we demonstrate below how the quantities  $I$  and  $\Gamma_{\text{exp}}$  are explained under these assumptions.

### A. Interpretation of the peak intensity

First, we consider how the peak luminescence intensity is determined. In our experiment, the absorptivity at the excitation photon energy was adjusted in a range 47–92%, and the absorbed energy by the samples coincide within a factor 2 for all metal samples. The absorbed energy is definitely transferred to the electron system because no other elementary excitation is expected in this energy region. The initial electron number generated in the metal is nearly the same

for all metals. In addition, the emissivity is common for all samples within a factor of 2. Therefore, the 300 times difference in the luminescence intensity at 0.9 eV among the metals should be ascribed to the different nonthermal electron dynamics before radiation of luminescence. In metals, electrons lose energy through e-ph interaction far faster than radiation process. This is one of the reasons why the quantum efficiency of luminescence in metal is very low under continuous wave (CW) excitation. However, the e-e scattering is an even faster process to reduce the nonthermal component, and it can be a mechanism of quenching the luminescence. In the following, we propose a model to interpret the intensity of the quasi-instantaneous component of luminescence. Here, we demonstrate that e-e scattering is relevant to the luminescence dynamics at the early stage of relaxation and that the peak luminescence intensity is determined by the inverse of the Drude damping rate.

Let us suppose a metal at a very low temperature as an initial state and photoexcitation by an infinitely short light pulse. The electron population just after photoexcitation is given by Eq. (3), showing that electrons with very high energy on the order of 1 eV exist.

We define the quantum yield of luminescence for the electron in an energy window  $\Delta E$  at  $E$  as

$$Y(E) = \frac{\Gamma_r}{\Gamma_r + \Gamma_{\text{nr}}(E)}, \quad (4)$$

where  $\Gamma_r$  is the radiative decay rate and assumed constant. Here,  $\Gamma_{\text{nr}}(E)$  is the nonradiative decay rate, which is strongly dependent on  $E$ , as will be discussed below. Here, the quantum yield is the number ratio of emitted photons to electrons generated in this energy window defined by  $\Delta E$ . Since the nonradiative decay rate is far larger than that of the radiative decay process in metals, Eq. (4) reduces to

$$Y(E) = \frac{\Gamma_r}{\Gamma_{\text{nr}}(E)}. \quad (5)$$

The nonradiative decay process, in other words, depopulation of the electrons from the energy window  $\Delta E$ , is caused by e-e and e-ph scattering. After single collision with other electrons, the nonthermal electrons lose a large amount of energy, while the energy loss due to e-ph scattering is on the order of the phonon energy, which is rather small. Therefore, e-e scattering is expected to be dominant in the decay process.

The relaxation of photoexcited high-energy electrons has been studied by means of time-resolved two-photon photoemission spectroscopy (2PPE) [28]. In most metals, it has been verified that the lifetime is nearly proportional to  $(E - E_F)^{-2}$ , as Fermi liquid theory predicts [29,30]. This means that the lifetime is dominated by e-e scattering. Lifetimes at 0.5 eV above  $E_F$  lie between 100 and 5 fs for many metals, whereas the lifetime is exceptionally long in Au (180 fs) due to the screening by  $d$  electrons. The 2PPE results support the dominance of e-e scattering for the decay of nonthermal electron.

The most probable radiative process for the electron at energy  $E$  is the recombination with holes just above  $E_F$  because the hole population is close to unity above  $E_F$ , and the spontaneous radiation probability is proportional to the square of the transition energy. Therefore,  $Y(E)$  approximately represents the intensity of the quasi-instantaneous component at

a photon energy  $E - E_F$ . Therefore, we can conclude that the intensity of the quasi-instantaneous luminescence is inversely proportional to the e-e scattering rate, as given by Eq. (5). Here, we should note that the experimentally obtained intensity of the quasi-instantaneous luminescence is the photon number counted within the time window of the time resolution (typically 0.24 ps), which is far larger than the lifetime of the instantaneous luminescence. Of course, the total energy of the electron system is conserved under the e-e scattering processes. In contrast, the decay of the exponential component is attributed to the cooling of the thermalized electrons via phonon emission, giving rise to overall energy loss of the electron system, as discussed in the following section.

Having established the relevance of the e-e scattering in the quasi-instantaneous luminescence, we next discuss the peak intensity  $I$ . As discussed, nonthermal electrons are responsible for  $I$ . In other words, if the e-e scattering rate is very fast, the electron quasiequilibrium is established instantaneously, giving rise to small  $I$ . Ideally, the evolution of electron distribution due to the e-e scattering should be studied by the Boltzmann transport equation [11,31–33]. However, it is not easy to study the relaxation dynamics based on a theoretical model by considering material-dependent properties such as electronic band structure and intraband transition rate. Alternatively, we propose a semiempirical approach based on the existing experimental information on the dielectric property of metals. By assuming dispersive media, we calculate the dissipation rate of electric field energy corresponding to frequency  $\omega$  [34,35]:

$$\gamma(\omega) = 2\varepsilon_2(\omega) \left[ \frac{\partial \varepsilon_1(\omega)}{\partial \omega} \right]^{-1}, \quad (6)$$

where  $\varepsilon_1(\omega)$  and  $\varepsilon_2(\omega)$  are the real and imaginary parts of the frequency-dependent dielectric function of a metal at a frequency  $\omega$ . This expression is also used to describe the damping rate of the plasmon mode in metal nanostructures [35]. Furthermore, this is consistent with the Drude formula [35]. In fact, by substituting the expression of  $\varepsilon = \varepsilon_\infty - \omega_p^2/(\omega^2 + i\omega\gamma_D)$  into Eq. (6), where  $\varepsilon_\infty$  is the dielectric constant at the high-frequency limit,  $\omega_p$  is the bulk plasmon frequency, and  $\gamma_D$  is the  $\omega$ -independent Drude damping rate, one obtains  $\gamma = \gamma_D$ . In this sense, we can regard  $\gamma$  in Eq. (6) as the Drude damping rate that reflects several scattering processes. Of course, the e-e scattering should be dominant in the quasi-instantaneous response, as discussed above.

To calculate  $\gamma$  for 15 elemental metals, we extracted the experimental data of the  $\omega$ -dependent refractive indices,  $n$  and  $k$ , from the refractiveindex.info database [36]. To interpolate the discrete data points, the  $\omega$  dependence of the dielectric constant was calculated by using a cubic spline algorithm. Figure 5 shows the luminescence intensity  $I(0.9 \text{ eV})$  as a function of  $1/\gamma(0.9 \text{ eV})$  for 15 elemental metals. The noble metals have a small damping rate (large  $1/\gamma$ ), which prevents ultrafast relaxation of nonthermal electrons. Therefore, they exhibit strong brightness (large  $I$ ). The  $1/\gamma$  exhibits a large variation among different metals. The  $1/\gamma$ 's of noble metals and Ti, Ni, and W differ by  $>100$  times and have a strong correlation with  $I$ . In addition, 11 metals (except Zn, Mg, and Ni) are distributed within the  $\sqrt{10}$  tolerance limits of the solid line, and three exceptions (Zn, Mg, and Ni) are located

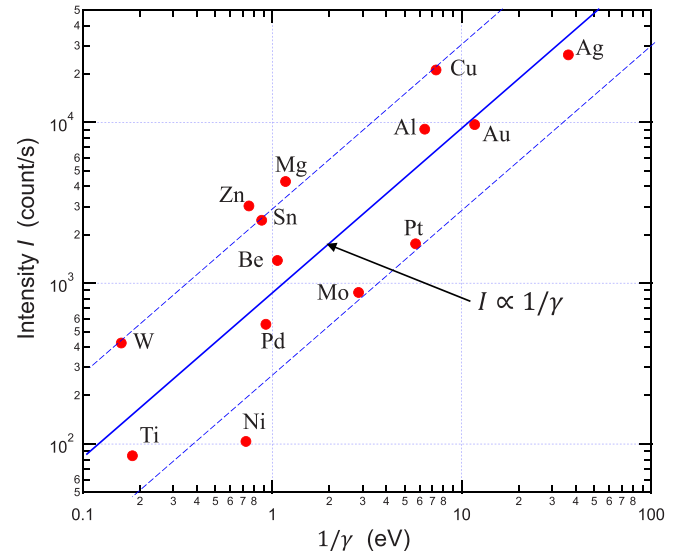


FIG. 5. Correlation between luminescence intensity  $I$  at 0.9 eV and  $1/\gamma$  calculated by Eq. (6). The solid straight line shows the  $I \propto 1/\gamma$  relation. The dashed lines show the  $\sqrt{10}$  tolerance limits. Zirconium (Zr) is omitted because  $\partial \varepsilon_1/\partial \omega < 0$  at 0.9 eV.

close to the tolerance lines. This simple model is sufficient to explain the general trend of the luminescence intensity of metals. As mentioned,  $I$  reflects the population of nonthermal electrons within the time resolution of the measurement, so that we evaluated  $\gamma$  at  $\hbar\omega = 0.9 \text{ eV}$ . Luminescence from electrons before e-e scattering is also found in gold flakes under CW excitation and is referred to as prescattering emission [15].

## B. Interpretation of the exponential decay rate

Next, we consider the luminescence decay rate  $\Gamma_{\text{exp}}$  that describes the electron-cooling rate after the electron temperature is almost established. We emphasize that  $\Gamma_{\text{exp}}$  is different from  $\gamma$  that describes the quasi-instantaneous response dominated by e-e scattering. We calculated the cooling rate due to the e-ph scattering by utilizing the theory developed by Kabanov and Alexandrov (KA) [37,38]:

$$\Gamma_{\text{KA}} = \frac{3\hbar\lambda\langle\Omega^2\rangle}{2\pi k_B T_{\text{ph}}}, \quad (7)$$

where  $\hbar$  is the Planck constant, and  $T_{\text{ph}}$  is phonon temperature, which is set to room temperature because the heat capacity of the lattice is large, and the transient increase of the lattice temperature is not significant in our experimental condition. The e-ph coupling strength is given by

$$\lambda\langle\Omega^n\rangle = 2 \int \alpha^2 F(\Omega) \Omega^{n-1} d\Omega, \quad (8)$$

where  $\alpha^2 F(\Omega)$  is the Eliashberg function at the phonon frequency  $\Omega$ , and  $n$  is an integer. This is the phonon DOS weighted by the e-ph matrix elements. For 15 metals, we computed  $\alpha^2 F(\Omega)$  based on density functional perturbation theory implemented in the QUANTUM ESPRESSO code [39]. The computational details are provided in the Supplemental Material [24].

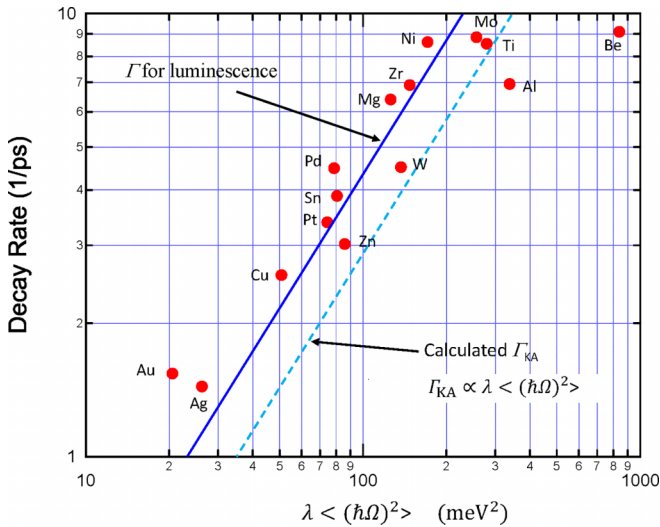


FIG. 6. Correlation between exponential decay rate  $\Gamma_{\text{exp}}$  at 0.6 eV and electron-phonon coupling constant. The blue dashed line represents the values calculated by Eq. (7). The values multiplied by 1.5 are shown by a solid line.

Equation (7) is derived using a linearized Boltzmann transport equation and treating the nonequilibrium component of the electron distribution as a perturbation [37]. In this sense, Eq. (7) is applicable even when the e-e collision rate is lower than the e-ph collision rate. This is different from the relaxation rate in an ordinary two-temperature model [40], where the e-e collision rate is assumed to be large enough to establish an electron quasiequilibrium at any time. Here,  $\Gamma_{\text{KA}}$  is linearly proportional to  $\lambda\langle\Omega^2\rangle$ . This relationship has been used to understand the transient optical responses of elemental metals [38], superconductors [41], and nanostructures [42].

Figure 6 shows  $\Gamma_{\text{exp}}$  in experiment vs  $\lambda\langle(\hbar\Omega)^2\rangle$ . The blue dashed line represents  $\Gamma_{\text{KA}}$  calculated from Eqs. (7) and (8), using the computed Eliashberg function. The experimental trends are explained well by the linear dependence. It is noteworthy that even the absolute value is close to those of experiment.

However, we notice a systematic upward shift of the experimental points in Fig. 6. This is because the parameter  $\Gamma_{\text{KA}}$  corresponds to the relaxation rate of macroscopic quantity such as excess electron energy or electron temperature, while  $\Gamma_{\text{exp}}$  is the decay rate of population observed at a fixed energy. To show this, we calculate a population decay at a fixed energy (0.6 eV) by assuming that the electron distribution is in quasiequilibrium and the electron temperature decays at a rate  $\Gamma_{\text{KA}}$ . As shown in the inset of Fig. 3, the decay rate of the electron population at 0.6 eV near the time origin is faster than  $\Gamma_{\text{KA}}$ , for the typical initial condition  $k_B T_0 = 0.24$  eV, where  $T_0$  is the initial electron temperature [21].

The overestimation of  $\Gamma_{\text{KA}}$  in Al and Be can be attributed to an implicit assumption in the theoretical model. The derivation of  $\Gamma_{\text{KA}}$  assumes that the phonon system is characterized by a single temperature [37]. However, the phonon distribution becomes a nonequilibrium one, if the  $\Omega$  dependence of  $\alpha^2 F(\Omega)$  is strong and the equilibration process within the

phonon system is slow (i.e., weak phonon-phonon scattering rates). In such a case, the temperature of some specific phonon modes increases, and electron cooling is hindered. This kind of phenomenon is often observed in semiconductors and is known as the *hot phonon effect* [43–45]. In fact, this was observed in Al, where electrons coupled with longitudinal phonons yielded different temperatures for the longitudinal and transverse phonons [46]. We consider that a similar scenario holds for Be: The Debye frequency is exceptionally large ( $\sim 20$  THz) [47], and  $\alpha^2 F(\Omega)$  in the high-frequency regime is relatively larger than in the low-frequency regime (see Fig. S4 in the Supplemental Material [24]), which may hinder the decay of high-frequency phonons into lower phonon modes.

## V. CONCLUSIONS

The lifetimes and intensities of the luminescence of 15 elemental metals were investigated using femtosecond luminescence spectroscopy, and the time profile of the luminescence was decomposed into quasi-instantaneous and exponential decay components. The variation of the intensity of the quasi-instantaneous component  $I$  among 15 elements was well understood in terms of a model based on two assumptions, i.e., (1) the instantaneous luminescence intensity is inversely proportional to nonradiative decay rate of the nonthermal electrons, and (2) a steady state is established between nonthermal and/or thermal electrons and the SPP. It was shown that the luminescence intensity  $I$  was proportional to the inverse of the Drude damping constant  $\gamma$  evaluated from the dielectric functions. It is worth noting that the ultrafast phenomena can be understood in terms of well-known classical parameters of metals. In other words, the luminescence data provide a microscopic verification of the Drude damping, in which all types of scatterings such as e-e, e-ph, and e-defect collisions are included. In this paper, we suggest that the Drude damping is dominated by the e-e scattering at least for the infrared regime. Assumption (1) can be replaced by a direct determination of the fast component of the luminescence with measurements with higher time resolution. It would, in principle, be possible because a time resolution of 40 fs was demonstrated in the visible region [48]. As for the verification of assumption (2), rigorous theoretical work describing the radiation from the excited-electron-SPP coupled system is required.

The exponentially decaying component was attributed to the cooling of thermal electrons via phonon emission, and the decay rates were found to be proportional to the e-ph coupling strength from *ab initio* calculations. Even the absolute values are in good agreement with experiment. This in turn shows that the luminescence method is usable for determining fundamental material constants, which are important for superconductivity theory, for example.

To summarize, in this paper, we highlight the fact that the underlying physics behind the infrared luminescence of metals with heavily roughened surface is governed by a complex interplay between hot carriers, phonons, and the SPP. We have demonstrated that the relationships  $I \propto 1/\gamma$  (Fig. 5) and  $\Gamma_{\text{exp}} \propto \lambda\langle\Omega^2\rangle$  (Fig. 6) are satisfied for most of the 15 metals,

providing a unified simple picture for the luminescence of metals.

At the end of this paper, we want to emphasize that our study of many kinds of metals with nearly equivalent geometry made it possible to reveal underlying physics of metal luminescence. This is in contrast with foregoing studies, in which authors were mostly concentrated on single metal (mainly noble metals) and specialized geometry such as nanodots, rods, flakes, or flowers.

*Note added.* We note an independent theoretical work discussing the luminescence of metals under CW excitations, introducing the generalized Kirchhoff's law [49].

## ACKNOWLEDGMENTS

We thank Prof. A. Sugita for useful discussion. This paper was supported by JSPS KAKENHI (Grant No. JP20K03823). T.S. is indebted to the Institute for Solid State Physics at the University of Tokyo for its support with the Joint Research Program. Some of the numerical calculations were done using the facilities of the Supercomputer Center, the Institute for Solid State Physics, the University of Tokyo, and the supercomputer MASAMUNE-IMR at the Center for Computational Materials Science, Institute for Materials Research, Tohoku University.

- 
- [1] A. Mooradian, Photoluminescence of metals, *Phys. Rev. Lett.* **22**, 185 (1969).
- [2] G. T. Boyd, Z. H. Yu, and Y. R. Shen, Photoinduced luminescence from the noble metals and its enhancement on roughened surfaces, *Phys. Rev. B* **33**, 7923 (1986).
- [3] T. Suemoto, S. Ono, A. Asahara, T. Okuno, T. Suzuki, K. Okazaki, S. Tani, and Y. Kobayashi, Observation of infrared interband luminescence in magnesium by femtosecond spectroscopy, *J. Appl. Phys.* **134**, 163105 (2023).
- [4] M. R. Beversluis, A. Bouhelier, and L. Novotny, Continuum generation from single gold nanostructures through near-field mediated intraband transitions, *Phys. Rev. B* **68**, 115433 (2003).
- [5] K. Imura, T. Nagahara, and H. Okamoto, Near-field two-photon-induced photoluminescence from single gold nanorods and imaging of plasmon modes, *J. Phys. Chem. B* **109**, 13214 (2005).
- [6] M. Hu, J. Chen, Z.-Y. Li, L. Au, G. V. Hartland, X. Li, M. Marquez, and Y. Xia, Gold nanostructures: Engineering their plasmonic properties for biomedical applications, *Chem. Soc. Rev.* **35**, 1084 (2006).
- [7] J. Zheng, C. Zhou, M. Yu, and J. Liu, Different sized luminescent gold nanoparticles, *Nanoscale* **4**, 4073 (2012).
- [8] L. Zhang and E. Wang, Metal nanoclusters: New fluorescent probes for sensors and bioimaging, *Nano Today* **9**, 132 (2014).
- [9] J. Khurgin, Hot carriers generated by plasmons: Where are they generated and where do they go from there? *Farad. Discuss.* **214**, 35 (2019).
- [10] J. Mertens, M-E. Kleemann, R. Chikkaraddy, P. Narang, and J. J. Baumberg, How light is emitted by plasmonic metals, *Nano Lett.* **17**, 2568 (2017).
- [11] Y. Sivan, I. W. Un, I. Kalyan, K-Q. Lin, J. M. Lupton, and S. Bange, Crossover from nonthermal to thermal photoluminescence from metals excited by ultrashort light pulses, *ACS Nano* **17**, 11439 (2023).
- [12] S. Ono and T. Suemoto, Ultrafast photoluminescence in metals: Theory and its application to silver, *Phys. Rev. B* **102**, 024308 (2020).
- [13] A. Tcherniak, S. Dominguez-Medina, W.-S. Chang, P. Swanglap, L. S. Slaughter, C. F. Landes, and S. Link, One-photon plasmon luminescence and its application to correlation spectroscopy as a probe for rotational and translational dynamics of gold nanorods, *J. Phys. Chem. C* **115**, 15938 (2011).
- [14] Y.-Y. Cai, J. G. Liu, L. J. Tauzin, D. Huang, E. Sung, H. Zhang, A. Joplin, W.-S. Chang, P. Nordlander, and S. Link, Photoluminescence of gold nanorods: Purcell effect enhanced emission from hot carriers, *ACS Nano* **12**, 976 (2018).
- [15] A. R. Bowman, A. R. Echarri, F. Kiani, F. Iyikanat, T. V. Tsoulos, J. D. Cox, R. Sundararaman, F. J. García de Abajo, and G. Tagliabue, Quantum mechanical effects in photoluminescence from thin crystalline gold films, *Light Sci. Appl.* **13**, 91 (2024).
- [16] T. Haug, P. Klemm, S. Bange, and J. M. Lupton, Hot-electron intraband luminescence from single hot spots in noble-metal nanoparticle films, *Phys. Rev. Lett.* **115**, 067403 (2015).
- [17] H. Kawasaki, H. Yamamoto, H. Fujimori, R. Arakawa, M. Inada, and Y. Iwasaki, Surfactant-free solution synthesis of fluorescent platinum subnanoclusters, *Chem. Commun.* **46**, 3759 (2010).
- [18] J. G. Fernández, L. Trapiella-Alfonso, M. J., R. Pereiro Costa-Fernández, and A. Sanz-Medel, Aqueous synthesis of near-infrared highly fluorescent platinum nanoclusters, *Nanotechnology* **26**, 215601 (2015).
- [19] M. Adelt, S. Nepijko, W. Drachsel, and H.-J. Freund, Size-dependent luminescence of small palladium particles, *Chem. Phys. Lett.* **291**, 425 (1998).
- [20] M. Hyotanishi, Y. Isomura, H. Yamamoto, H. Kawasaki, and Y. Obora, Surfactant-free synthesis of palladium nanoclusters for their use in catalytic cross-coupling reactions, *Chem. Commun.* **47**, 5750 (2011).
- [21] T. Suemoto, K. Yamanaka, N. Sugimoto, Y. Kobayashi, T. Otsu, S. Tani, and T. Koyama, Relaxation dynamics of hot electrons in the transition metals Au, Ag, Cu, Pt, Pd, and Ni studied by ultrafast luminescence spectroscopy, *J. Appl. Phys.* **130**, 025101 (2021).
- [22] T. Suemoto, K. Yamanaka, N. Sugimoto, T. Otsu, S. Tani, Y. Kobayashi, and T. Koyama, Effect of emissivity on ultrafast luminescence spectra in silver, *J. Appl. Phys.* **128**, 203103 (2020).
- [23] T. Suemoto, K. I. Yamanaka, and N. Sugimoto, Observation of femtosecond infrared luminescence in gold, *Phys. Rev. B* **100**, 125405 (2019); **104**, 119905(E) (2021).
- [24] See Supplemental Material at <http://link.aps.org/supplemental/10.1103/PhysRevB.111.035150> for the time evolution of the luminescence intensity for the elements not included in Figs. 1 and 2, time-resolved luminescence spectra for 15 metals, and the computational details for e-ph coupling (see also Refs. [50–53] therein).
- [25] P. Nagpal, N. C. Lindquist, S. H. Oh, and D. J. Norris, Ultrasmooth patterned metals for plasmonics and metamaterials, *Science* **325**, 594 (2009).

- [26] N. Hiramatsu, F. Kusa, K. Imasaka, I. Morichika, A. Takegami, and S. Ashihara, Propagation length of mid-infrared surface plasmon polaritons on gold: Impact of morphology change by thermal annealing, *J. Appl. Phys.* **120**, 173103 (2016).
- [27] W. L. Barnes, A. Dereux, and T. W. Ebbesen, Surface plasmon subwavelength optics, *Nature (London)* **424**, 824 (2003).
- [28] M. Bauer, A. Marienfeld, and M. Aeschlimann, Hot electron lifetimes in metals probed by time-resolved two-photon photoemission, *Prog. Surf. Sci.* **90**, 319 (2015).
- [29] E. Zarate, P. Apell, and P. M. Echenique, Calculation of low-energy-electron lifetimes, *Phys. Rev. B* **60**, 2326 (1999).
- [30] V. P. Zhukov, F. Aryasetiawan, E. V. Chulkov, and P. M. Echenique, Lifetimes of quasiparticle excitations in *4d* transition metals: Scattering theory and LMTO-RPA-GW approaches, *Phys. Rev. B* **65**, 115116 (2002).
- [31] B. Y. Mueller and B. Rethfeld, Relaxation dynamics in laser-excited metals under nonequilibrium conditions, *Phys. Rev. B* **87**, 035139 (2013).
- [32] S. Ono, Thermalization in simple metals: Role of electron-phonon and phonon-phonon scattering, *Phys. Rev. B* **97**, 054310 (2018).
- [33] Y. Sivan and Y. Dubi, Theory of “hot” photoluminescence from Drude metals, *ACS Nano* **15**, 8724 (2021).
- [34] L. D. Landau and E. M. Lifshitz, *Electrodynamics of Continuous Media* (Elsevier, Amsterdam, 2004).
- [35] A. S. Kirakosyan, M. I. Stockman, and T. V. Shahbazyan, Surface plasmon lifetime in metal nanoshells, *Phys. Rev. B* **94**, 155429 (2016).
- [36] M. N. Polyanskiy, Refractiveindex.info database of optical constants, *Sci. Data* **11**, 94 (2024).
- [37] V. V. Kabanov and A. S. Alexandrov, Electron relaxation in metals: Theory and exact analytical solutions, *Phys. Rev. B* **78**, 174514 (2008).
- [38] M. Oberfell and J. Demsar, Tracking the time evolution of the electron distribution function in copper by femtosecond broadband optical spectroscopy, *Phys. Rev. Lett.* **124**, 037401 (2020).
- [39] P. Giannozzi, O. Andreussi, T. Brumme, O. Bunau, M. B. Nardelli, M. Calandra, R. Car, C. Cavazzoni, D. Ceresoli, M. Cococcioni, N. Colonna, I. Carnimeo, A. Dal Corso, S. de Gironcoli, P. Delugas, R. A. DiStasio Jr, A. Ferretti, A. Floris, G. Fratesi, G. Fugallo *et al.*, Advanced capabilities for materials modeling with QUANTUM ESPRESSO, *J. Phys.: Condens. Matter* **29**, 465901 (2017).
- [40] P. B. Allen, Theory of thermal relaxation of electrons in metals, *Phys. Rev. Lett.* **59**, 1460 (1987).
- [41] C. Gadermaier, A. S. Alexandrov, V. V. Kabanov, P. Kusar, T. Mertelj, X. Yao, C. Manzoni, D. Brida, G. Cerullo, and D. Mihailovic, Electron-phonon coupling in high-temperature cuprate superconductors determined from electron relaxation rates, *Phys. Rev. Lett.* **105**, 257001 (2010).
- [42] S. Ono, Y. Toda, and J. Onoe, Unified understanding of the electron-phonon coupling strength for nanocarbon allotropes, *Phys. Rev. B* **90**, 155435 (2014).
- [43] M. C. Tatham, J. F. Ryan, and C. T. Foxon, Time-resolved Raman measurements of intersubband relaxation in GaAs quantum wells, *Phys. Rev. Lett.* **63**, 1637 (1989).
- [44] D. S. Kim and P. Y. Yu, Hot-electron relaxations and hot phonons in GaAs studied by subpicosecond Raman scattering, *Phys. Rev. B* **43**, 4158 (1991).
- [45] P. Langot, N. Del Fatti, D. Christofilos, R. Tommasi, and F. Vallée, Femtosecond investigation of the hot-phonon effect in GaAs at room temperature, *Phys. Rev. B* **54**, 14487 (1996).
- [46] L. Waldecker, R. Bertoni, R. Ernstorfer, and J. Vorberger, Electron-phonon coupling and energy flow in a simple metal beyond the two-temperature approximation, *Phys. Rev. X* **6**, 021003 (2016).
- [47] R. Stedman, Z. Amilius, R. Pauli, and O. Sundin, Phonon spectrum of beryllium at 80 K, *J. Phys. F: Met. Phys.* **6**, 157 (1976).
- [48] T. Matsuoka, S. Saito, J. Takeda, S. Kurita, and T. Suemoto, Overtone modulation and anti-phasing behavior of wave-packet amplitudes on the adiabatic potential surface of self-trapped excitons, *Nonlinear Optics* **29**, 587 (2002).
- [49] A. Loirette-Pelous and J.-J. Greffet, Theory of photoluminescence by metallic structures, *ACS Nano* **18**, 31823 (2024).
- [50] M. Methfessel and A. T. Paxton, High-precision sampling for Brillouin-zone integration in metals, *Phys. Rev. B* **40**, 3616 (1989).
- [51] J. P. Perdew, K. Burke, and M. Ernzerhof, Generalized gradient approximation made simple, *Phys. Rev. Lett.* **77**, 3865 (1996).
- [52] J. P. Perdew, A. Ruzsinszky, G. I. Csonka, O. A. Vydrov, G. E. Scuseria, L. A. Constantin, X. Zhou, and K. Burke, Restoring the density-gradient expansion for exchange in solids and surfaces, *Phys. Rev. Lett.* **100**, 136406 (2008).
- [53] S. Baroni, S. Gironcoli, A. Dal Corso, and P. Giannozzi, Phonons and related crystal properties from density-functional perturbation theory, *Rev. Mod. Phys.* **73**, 515 (2001).